Available online at www.sciencedirect.com
ScienceDirect
Acta Materialia 58 (2010) 39–48
Acta MATERIALIA
www.elsevier.com/locate/actamat

Effect of space charge on the polarization hysteresis characteristics of monolithic and compositionally graded ferroelectrics

M.B. Okatan [a], J.V. Mantese [b], S.P. Alpay [a,*]

[a] Materials Science and Engineering Program, Department of Chemical, Materials, and Biomolecular Engineering, University of Connecticut, Storrs, CT 06269, United States
[b] United Technologies Research Center, East Hartford, Storrs, CT 06108, United States

Received 23 May 2009; received in revised form 13 August 2009; accepted 26 August 2009
Available online 24 September 2009

Abstract

A non-linear thermodynamic analysis of ferroelectric systems with localized space charges for monolithic and compositionally graded materials is described wherein the electrostatic interlayer interactions are specifically accounted for. The electrostatic coupling is established through the built-in polarization due to the space charges and the intrinsic polarization variations between the ferroelectric layers. The findings show that the polarization hysteresis response of monolithic stress-free barium strontium titanate (BST) ferroelectrics with asymmetrically distributed space charges result in a displacement of the hysteresis loop along the applied electric field axis. In compositionally graded BST multilayers, the hysteresis response is characterized by off-sets along both the polarization and the electric field axes, yet with magnitudes of displacement that are markedly larger than those for monolithic ferroelectrics.
Published by Elsevier Ltd. on behalf of Acta Materialia Inc.

Keywords: Dielectrics; Multilayers; Perovskites; Ferroelectricity; Interface defects

1. Introduction

It has been nearly 20 years since the observation of a displacement of the polarization–electric field hysteresis loop along the polarization axis and a giant (pseudo) pyroelectric response in a compositionally graded $KNbO_3$–$KTaO_3$ and the postulation that its origin arises from an intrinsic potential as a result of the concentration gradient [1]. Since that time, there has been significant interest in ferroelectric heterostructures with asymmetric variations in the composition. Much of the discussion in the literature has sought to clarify whether the initial findings were of a fundamental nature, with potential for a new class of solid-state devices or an artifact arising from imperfect chemistry or crystallinity.

While similar behavior was observed in other ferroelectric systems, including those in Refs. [2–9], the controversy surrounding graded ferroelectrics has remained mainly unresolved. Experimental studies are intriguing, in that they show graded ferroelectrics give a temperature insensitive dielectric response and tunability [10,11], as well as an exceptionally large pyroelectric response [1]. In addition to these findings, it has also been noted that similar polarization off-sets have been observed experimentally by impressing temperature gradients or by imposing nonuniform external stress fields across a monolithic ferroelectric material lending credibility to a fundamental root cause to the phenomenon [12,13].

Various theoretical approaches have been proposed in order to explain the origin of the polarization off-sets. One mechanism strongly argued for is that the off-sets arise from asymmetrical current injection at the contacts [14], while others have proposed time-dependent space-charge-limited conduction [15]; plausible lines of reasoning as such behavior has often been reported for imperfect

* Corresponding author. Address: Materials Science and Engineering Program, Department of Chemical, Materials, and Biomolecular Engineering, University of Connecticut, 97 N. Eagleville Road, U-3136, Storrs, CT 06269, United States.
E-mail address: p.alpay@ims.uconn.edu (S.P. Alpay).

1359-6454/$36.00 Published by Elsevier Ltd. on behalf of Acta Materialia Inc.
doi:10.1016/j.actamat.2009.08.055

semiconductor materials and imperfect contacts [16]. Traditional analysis has been complicated as well since the concentration, temperature or strain gradients imposed in the experiments have necessitated modification of the Landau–Ginzburg free energy with the introduction of a term in odd power of polarization [17]. A similar methodology can be employed to describe any systematic variation in other scalar quantities, such as defect concentration and density [18].

There have also been theoretical studies focusing on the modification of the properties of ferroelectric materials in the presence of space charges. Bratkovsky and Levanyuk [19] predicted a suppression of the ferroelectric–paraelectric phase transition temperature with increasing space charge density. Due to discretely distributed localized charges, a monolithic ferroelectric material can be thought of to be composed of "sections" or "layers" with different polarization values when space charges are present. Theoretical analysis clearly shows that polarization switching in each section or layer takes place at the same coercive electric field strength [19]. Building upon these results, Zubko et al. [20], found a reduction in the polarization and coercive electric field with increasing space charge densities and examined possible leakage mechanisms such as space-charge limited conduction, Schottky thermionic emission under full and partial depletion and Poole–Frenkel conduction [21]. Similar studies were carried out by Pintilie et al. [22]. These show that the leakage mechanisms in metal–ferroelectric–metal heterostructures can be related to interface controlled injection of charges followed by their slow drift through the film. Furthermore, recent models based on electrostatic interactions between ferroelectric multilayers [23] that take into account the presence of localized charge demonstrate that the overall polarization response may be enhanced due to the "built-in" polarization [24].

In this study, we present the results of a theoretical analysis that aims to combine the many effects and theories of compositionally graded and spatially localized charges at the interlayer interfaces. The formalism is based on Landau theory of phase transformations taking into consideration electrostatic interactions between layers originating from localized space charges and the polarization in each layer. Due to these electrostatic fields, we show that it is possible to displace the thermodynamic polarization hysteresis loops along both the polarization and the electric field axes. More interestingly, we find that, when a compositional gradient exists, even small amounts of localized space charges markedly accentuate the off-sets.

2. Theory

To understand the combined role of localized space charges at interlayer interfaces (specified through a surface charge density of σ) and compositional gradients, we begin our analysis by considering four different model cases: (i) a monolithic ferroelectric material free from space charges,

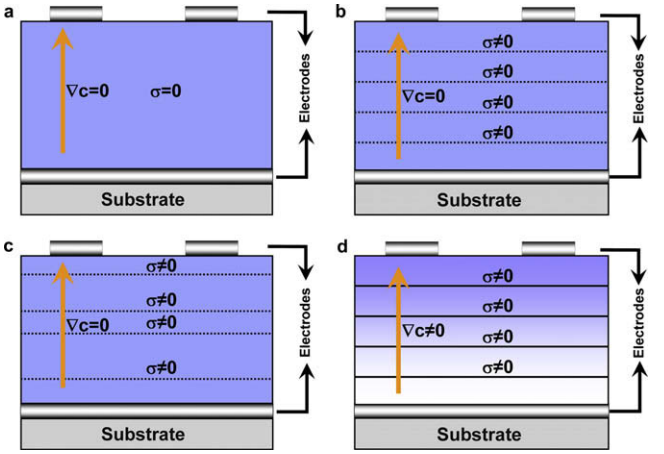

Fig. 1. (a) Monolithic ($\nabla_c = 0$) ferroelectric material free from space charges ($\sigma = 0$); (b) monolithic ferroelectric material consisting of "layers" of equal thickness with space charges located at each interlayer interface; (c) monolithic ferroelectric material consisting of "layers" with different thicknesses with space charges located at each interlayer interface; and (d) multilayered compositionally graded ($\nabla_c \neq 0$) ferroelectric heterostructure made up of layers of equal thickness with space charges located at each interlayer interface.

$\sigma = 0$ (Fig. 1a); (ii) a monolithic ferroelectric material in which space charges are distributed symmetrically with respect to the midsection of the ferroelectric material so that the ferroelectric material is divided into layers (sections) with equal thicknesses on which space charges are located (Fig. 1b); (iii) a monolithic ferroelectric material in which space charge ($\sigma \neq 0$) is distributed asymmetrically with respect to the midsection of the ferroelectric material, i.e. divided into layers having different thicknesses (Fig. 1c), hence the space charge is skewed towards either the top or the bottom electrode; and (iv) a multilayered compositionally graded ferroelectric heterostructure in which the space charge ($\sigma \neq 0$) is distributed symmetrically with respect to the midsection of the heterostructure, i.e. same layer thickness (Fig. 1d).

In all these cases, we assume that the ferroelectric film or each layer depending on the particular case (Fig. 1) is in a monodomain state. We note that for the compositionally graded heterostructure of Fig. 1d it is possible to form a polydomain state consisting of wedge-shaped domains to minimize the total electrostatic energy [25,26]. We further assume in our theoretical approach that the ferroelectric material is stress-free and unclamped so as to be able to isolate the effects of either the space charges or the compositional gradients on the resulting ferroelectric properties. The model can be readily expanded to thin film systems by taking into account epitaxial/thermal strains and the two-dimensional clamping of the substrate through renormalized Landau coefficients [27].

The electrostatic boundary conditions governing the electrical response of such kind of heterostructures are given by: (i) the continuity of the normal component of

the electric displacement field at each interlayer interface, i.e.

$$(P_i - P_{i+1}) + \varepsilon_0(E_{D,i} - E_{D,i+1}) = \sigma \quad i = 1, 2, \ldots, (n-1) \tag{1}$$

and (ii) the short-circuit conditions (both electrodes are held at the same potential),

$$\sum_{i=1}^{n} \ell_i E_{D,i} = 0 \tag{2}$$

Here, P_i, $E_{D,i}$ and ℓ_i are the polarization, depolarizing electric field in layer i and thickness of layer i, respectively, and ε_0 is the permittivity of free space. The polarization in each layer i is assumed to be constant. For the sake of simplicity, the localized surface charge density σ is taken to be constant in our calculations. Such a discrete allocation of localized charges is employed to approximate a continuous "homogeneous" distribution of space charges [19]. The condition of constant σ can certainly be relaxed to discuss more complicated cases although we shall refrain from doing so in this study. These include, for instance, non-monotonic variations in the charge density or a "lump" of charge concentrated at a particular interlayer interface. This can be achieved by assigning a different space charge density to each interlayer interface (σ_i) and/or varying the layer thicknesses. For example, in a recent study we analyzed the effects of polarization coupling in ferroelectric multilayers where the space charges are localized at each interlayer interface with different concentrations resulting in a uniform "coupling strength parameter" between layers in the heterostructure [28]. We shall show that "asymmetric" (nonhomogeneous) distribution of space charges may be achieved by varying the thickness of each "layer" (see Fig. 1c).

The solution of the system of equations given via relations (1) and (2) is described in the Appendix A. Accordingly,

$$E_{D,i} = -\frac{1}{\varepsilon_0}\left\{P_i - \sum_{j=1}^{n}\alpha_j P_j + \left[\sum_{j=1}^{n}(n-j)\alpha_j - (n-i)\right]\sigma\right\} \quad i = 1, 2, \ldots, n \tag{3}$$

Therefore, in the most general case, the total free energy density of an n-layered ferroelectric heterostructure is given as:

$$F_\Sigma = \sum_{i=1}^{n}\alpha_i\left(F_{0,i} + \frac{1}{2}a_i P_i^2 + \frac{1}{4}b_i P_i^4 + \frac{1}{6}c_i P_i^6 - E^{\text{ext}}P_i\right) - \frac{1}{2}\sum_{i=1}^{n}\alpha_i E_{D,i} P_i, \tag{4}$$

where α_i is the volume fraction of layer i, $F_{0,i}$ is the free energy density of the polarization-free paraelectric phase, and a_i, b_i, and c_i are the dielectric stiffness coefficients of layer i. The temperature dependence of the coefficient a_i is given by the CurieWeiss law such that $a_i = (T - T_{C,i})/\varepsilon_0 C_i$, where $T_{C,i}$ and C_i are the Curie temperature and constant of layer i, respectively. E^{ext} is the externally applied electric field.

Inserting Eq. (3) into Eq. (4) results in a term that encompasses an odd power of the polarization; $(\alpha_i\sigma/2\varepsilon_0)\left[\sum_{j=1}^{n}(n-j)\alpha_j - (n-i)\right]P_i$. This term behaves mathematically in an identical fashion to the phenomenological term suggested by Marvan and Fousek [17] and Bratkovsky and Levanyuk [18]. We shall show that this term will result in the displacement of the thermodynamic hysteresis loops of ferroelectrics with localized space charges and compositionally graded ferroelectric heterostructures.

The equilibrium polarizations, P_i, are determined as solutions to the equations of state given as $\partial F_\Sigma/\partial P_i = 0$ for $i = 1, 2, \ldots, n$ where

$$\frac{\partial F_\Sigma}{\partial P_i} = a_i P_i + b_i P_i^3 + c_i P_i^5 - E^{\text{ext}} + \frac{1}{\varepsilon_0}\left(P_i - \sum_{j=1}^{n}\alpha_j P_j\right) + \frac{\sigma}{2\varepsilon_0}\left[\sum_{j=1}^{n}(n-j)\alpha_j - (n-i)\right] \tag{5}$$

The average polarization $\langle P\rangle$ is calculated from the equilibrium polarizations:

$$\langle P\rangle = \sum_{i=1}^{n}\alpha_i P_i \tag{6}$$

The electric field, at which the determinant of the Hessian matrix of the total Gibbs free energy function F_Σ becomes zero (i.e. it looses its positive definiteness) is the thermodynamic coercive field. Formally, we look for an E^{ext} which results in

$$\begin{vmatrix} \frac{\partial^2 F_\Sigma}{\partial P_1^2} & \frac{\partial^2 F_\Sigma}{\partial P_1 \partial P_2} & \cdots & \frac{\partial^2 F_\Sigma}{\partial P_1 \partial P_{n-1}} & \frac{\partial^2 F_\Sigma}{\partial P_1 \partial P_n} \\ \frac{\partial^2 F_\Sigma}{\partial P_2 \partial P_1} & \frac{\partial^2 F_\Sigma}{\partial P_2^2} & \cdots & \frac{\partial^2 F_\Sigma}{\partial P_2 \partial P_{n-1}} & \frac{\partial^2 F_\Sigma}{\partial P_2 \partial P_n} \\ \vdots & \vdots & \ddots & \vdots & \vdots \\ \frac{\partial^2 F_\Sigma}{\partial P_{n-1} \partial P_1} & \frac{\partial^2 F_\Sigma}{\partial P_{n-1} \partial P_2} & \cdots & \frac{\partial^2 F_\Sigma}{\partial P_{n-1}^2} & \frac{\partial^2 F_\Sigma}{\partial P_{n-1} \partial P_n} \\ \frac{\partial^2 F_\Sigma}{\partial P_n \partial P_1} & \frac{\partial^2 F_\Sigma}{\partial P_n \partial P_2} & \cdots & \frac{\partial^2 F_\Sigma}{\partial P_n \partial P_{n-1}} & \frac{\partial^2 F_\Sigma}{\partial P_n^2} \end{vmatrix} = 0 \tag{7}$$

where

$$\frac{\partial^2 F_\Sigma}{\partial P_i^2} = \alpha_i(a_i + 3b_i P_i^2 + 5c_i P_i^4) + \frac{\alpha_i}{\varepsilon_0}(1 - \alpha_i) \tag{8}$$

$$\frac{\partial^2 F_\Sigma}{\partial P_i \partial P_j} = -\frac{\alpha_i \alpha_j}{\varepsilon_0} \tag{9}$$

and P_k denote the corresponding solutions of the system of equations at E^{ext} given via Eq. (5).

3. Results and discussion

In this study, we focused on the evolution of the hysteresis response of the four systems shown in Fig. 1. In order to describe the differences in the polarization–electric field hysteresis response of these systems, we provide in Fig. 2

a schematic representation of a displaced thermodynamic hysteresis loop. Fig. 2 also contains parameters that will be employed to characterize such hysteresis response. E_{cl} and E_{cr} are the coercive electric fields on the left and right side of the hysteresis loop, respectively. E_{hc} is the coordinate of the center of the hysteresis loop along the electric field axis, i.e. $E_{hc} = \frac{1}{2}(E_{cr} + E_{cl})$. H_w is the width of the hysteresis response, i.e. $H_w = E_{cr} - E_{cl}$. H_h is the height of the hysteresis loop such that $H_h = P^{up}(E_{hc}) - P^{down}(E_{hc})$ where $P^{up}(E_{hc})$ and $P^{down}(E_{hc})$ are the up (positive) and down (negative) polarizations at E_{hc}, respectively. P_{hc} is the coordinate of the center of the hysteresis loop along the polarization axis defined through $P_{hc} = \frac{1}{2}[P^{up}(E_{hc}) + P^{down}(E_{hc})]$.

For our simulations we considered barium strontium titanate, $Ba_xSr_{1-x}TiO_3$ [BST $x/(1-x)$], as the ferroelectric material. The thermodynamic parameters of BST were assumed to vary linearly as a function of x between those values of bulk $BaTiO_3$ and bulk $SrTiO_3$ listed in Table 1 [28].

3.1. Monolithic ferroelectric material

For a monolithic, stress-free, unclamped ferroelectric material free from space charges, i.e. $n = 1$ and $\sigma = 0$, shown in Fig. 1a, the total free energy given by Eq. (4) simplifies to the well-known relation:

$$F_\Sigma = F_0 + \frac{1}{2}aP^2 + \frac{1}{4}bP^4 + \frac{1}{6}cP^6 - E^{ext}P \qquad (10)$$

In Fig. 3 we plot the thermodynamic hysteresis loop of a monolithic ferroelectric BST 80/20 for which, quite expectedly, the center (E_{hc}, P_{hc}) is located at the origin (0, 0) of the polarization–electric field coordinate system.

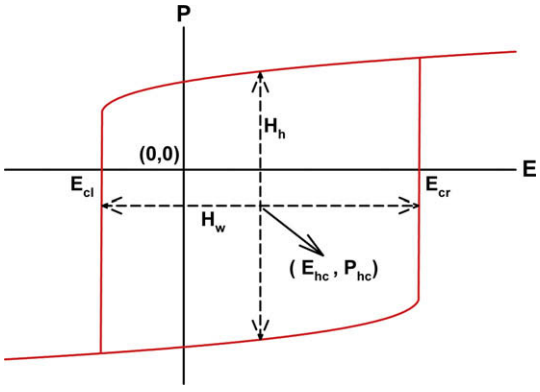

Fig. 2. Schematic drawing of a displaced hysteresis loop and the parameters employed to define the hysteresis response.

Table 1
Materials and thermodynamic parameters of bulk $BaTiO_3$ and $SrTiO_3$ (T in °C).

	T_C (°C)	C (°C)	b (Nm^6/C^4)	c (Nm^{10}/C^6)
$BaTiO_3$	120	1.7×10^5	$1.44\,(T - 175) \times 10^7$	3.96×10^{10}
$SrTiO_3$	−253	0.8×10^5	8.4×10^9	–

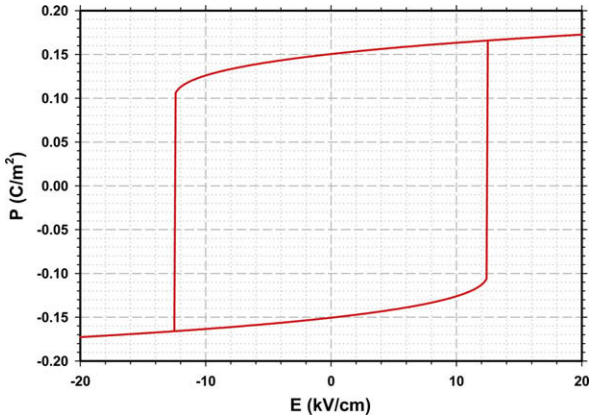

Fig. 3. Hysteresis loop of a charge-free BST 80/20 at room temperature shown in Fig. 1a. It is centered exactly at (0, 0).

3.2. Monolithic ferroelectric with symmetrically distributed space charges

In this case, the hysteresis loop shrinks progressively along both the electric and the polarization axis, i.e. both its width and height decrease with increasing space charge density. These results are consistent with the findings of Zubko et al. [20] for fully depleted films. This reduction can be clearly seen in Fig. 4, where the evolution of the hysteresis loop is determined as a function of the space charge density σ (from 0 to 0.1 C m^{-2}) viewed along the σ-axis for a BST 80/20 ferroelectric consisting of five equally thick layers. The most outer and inner hysteresis loops corresponds to $\sigma = 0$ and 0.1 C m^{-2}, respectively. The highlighted loop corresponds to $\sigma = 0.05$ C m^{-2}. The hysteresis loop remains centered exactly at the origin for all σ values investigated, i.e. (E_{hc}, P_{hc}) = (0, 0). The room temperature variations of all the hysteresis parameters with space charge density are provided in Fig. 5. At low values of space charge density ($\sigma \leqslant 0.02$ C m^{-2}) both the "right" and "left" coercive electric fields, and thus the width of

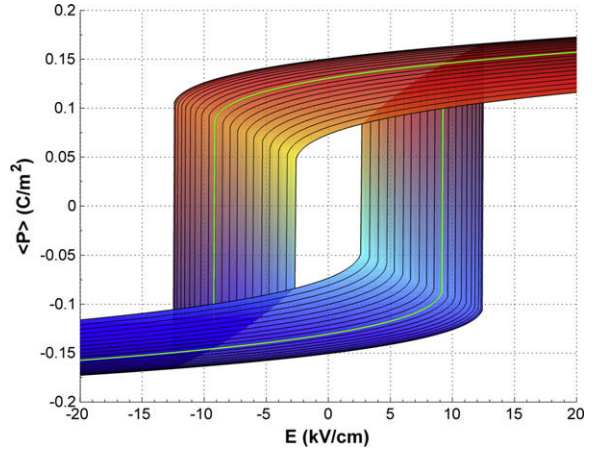

Fig. 4. Dependence of the hysteresis loop of BST 80/20 at room temperature on symmetrically distributed σ (Fig. 1b) with five equally thick "layers". It is centered exactly at (0, 0).

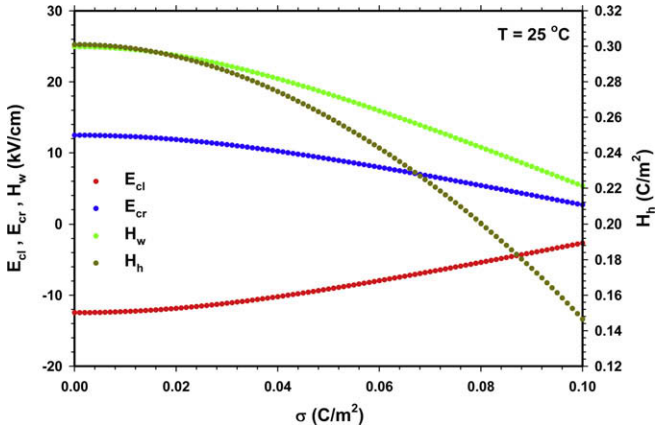

Fig. 5. Variation of hysteresis parameters of BST 80/20 at room temperature on symmetrically distributed σ (Fig. 1b) with five equally thick "layers".

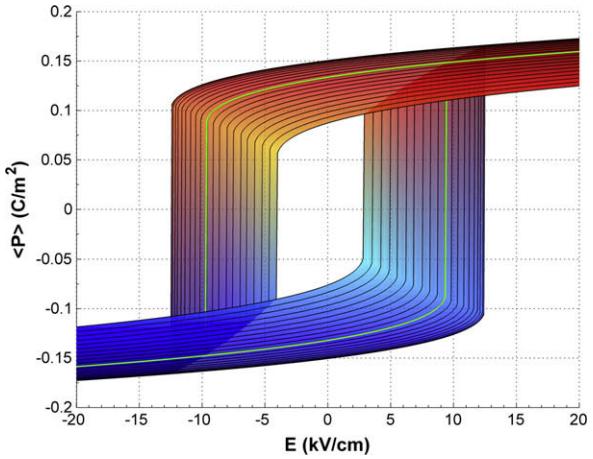

Fig. 6. Dependence of the hysteresis loop of BST 80/20 at room temperature with five "layers" on asymmetrically distributed σ (Fig. 1c) towards the top electrode for layer fractions 0.14, 0.34, 0.13, 0.23, and 0.16.

the hysteresis loop, remain practically unchanged. However, these parameters decrease approximately linearly toward zero with increasing space charge densities.

3.3. Monolithic ferroelectric with asymmetrically distributed space charges

In this case, the monolithic ferroelectric material can be thought of as if it were made up of layers of different thickness such that $\alpha_i \neq \alpha_j$, as shown schematically in Fig. 1c. Note that we consider here only configurations that will yield an asymmetric charge distribution. For such geometries, space charge accumulates on one side of the ferroelectric material and the charge distribution symmetry with respect to the midsection of the ferroelectric material is lost. We examined a distribution of space charges in a BST 80/20 ferroelectric where the volume fractions of layers were taken as 0.14, 0.34, 0.13, 0.23, and 0.16 from the bottom electrode to the top electrode. For this particular configuration, the space charge is skewed towards the top electrode. The variation of the hysteresis loop with space charge density σ is depicted in Fig. 6 along the σ-axis. The most outer and inner hysteresis loops correspond to $\sigma = 0$ and 0.1 C m^{-2}, respectively. The highlighted loop is for $\sigma = 0.05$ C m^{-2}. Again, as in the previous case, the primary effect of the space charges is to cause a contraction in the hysteresis loops. There is a negligible change in the hysteresis behavior for $\sigma < 0.02$ C m^{-2} (see Fig. 7a and b). Moreover, it is notable that for high space charge densities ($\sigma \geqslant 0.04$ C m^{-2}) the loops are clearly shifted along the electric field axis towards negative electric field values. Although this effect is small, it is not negligible and the displacement increases linearly with increasing space charge density. Such kind of shifts along the electric field axis have commonly been observed experimentally, and this behavior is usually explained through the presence of charged defects (see e.g. [29,30]). On the other hand, the shift along the polarization axis is minute, corresponding to variations on the order of 10^{-4} C m^{-2} (Fig. 7b). Thus, the center of

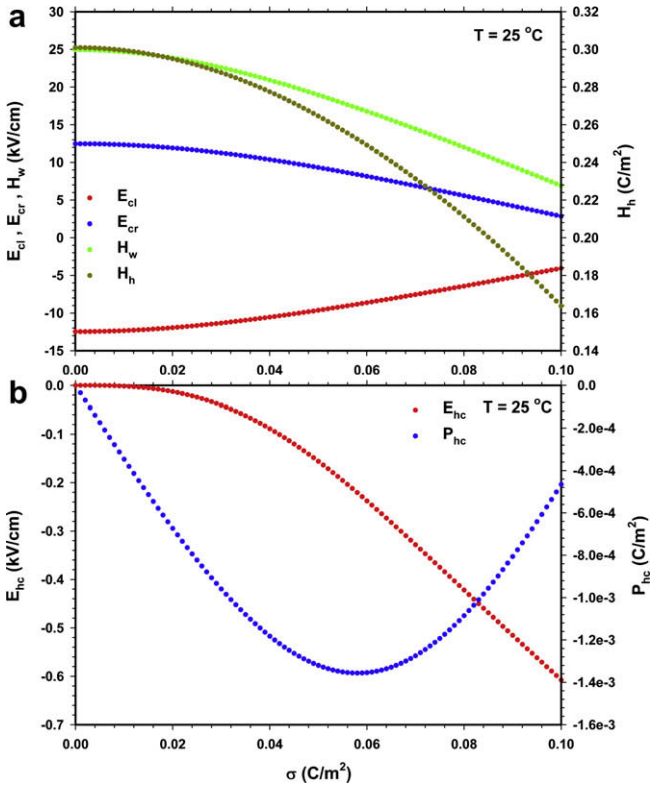

Fig. 7. Variation of hysteresis parameters of BST 80/20 at room temperature with five "layers" for asymmetrically distributed σ (Fig. 1c) towards the top electrode with layer fractions 0.14, 0.34, 0.13, 0.23, and 0.16.

the hysteresis loop is located on the electric field axis. Reversing the space charge distribution, i.e. changing the volume fractions of layers from bottom to top electrode as 0.16, 0.23, 0.13, 0.34, and 0.14, flips the direction of both of the shifts observed along the electric and the polarization axis (Fig. 8). In this case, the center of the hysteresis

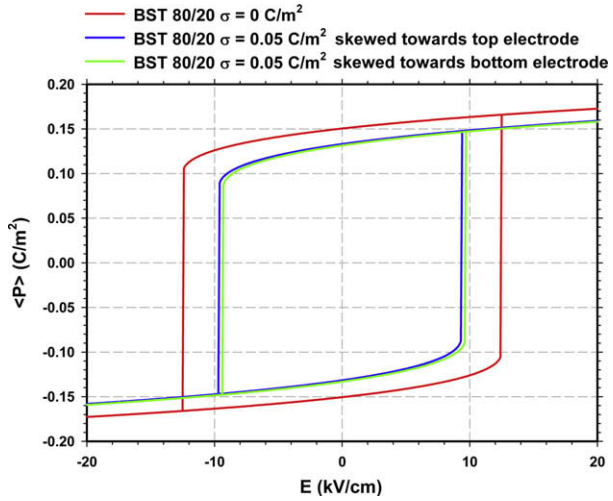

Fig. 8. Dependence of the hysteresis loop of BST 80/20 at room temperature with five "layers" on asymmetrically distributed σ (Fig. 1c). Layer fractions were taken as 0.14, 0.34, 0.13, 0.23, and 0.16 towards the top electrode and 0.16, 0.23, 0.13, 0.34, and 0.14 towards the bottom electrode.

loop (E_{hc}, P_{hc}) is translated to $(-E_{hc}, -P_{hc})$, which can be obtained by multiplying the values given in Fig. 7b by (-1).

3.4. Compositionally graded ferroelectric with symmetrically distributed space charges

We examined the effect of space charge on the hysteresis loop of a five-layered upgraded $Ba_xSr_{1-x}TiO_3$ [BST $x/(1-x)$] heterostructure in which from bottom to top electrode composition of each layer was taken as BST 70/30–75/25–80/20–85/15–90/10. Compared to the monolithic ferroelectrics with either symmetrically or asymmetrically distributed space charges, the presence of even small amounts of space charge in compositionally graded ferroelectrics has an immense effect on the hysteresis response for these systems, as shown in Fig. 9. The first striking feature is that the shift observed along the electric field axis is significantly larger than that of a monolithic ferroelectric with an asymmetric charge distribution; the hysteresis loops are displaced to the right with increasing space charge density, σ. The variation of the hysteresis parameters describing the loops as a function of σ are summarized in Fig. 10. It can be seen that, as in the previous cases of monolithic ferroelectrics, the hysteresis loops become smaller both in width and height with increasing σ. Note also, however, that there is now considerable displacement along the polarization axis as well (Fig. 10b). Therefore, the center of the hysteresis loop moves along a diagonal-like trajectory as a function of the space charge density. The direction of the movement of the center of the hysteresis loop depends on the direction of compositional grading, i.e. whether the ferroelectric is upgraded or downgraded. This is presented in Fig. 11, where it is shown that when going from an upgraded to a downgraded ferroelectric heterostructure the magnitude of the diagonal-like displacement is preserved but not its direction. For example, in a downgraded BST 90/10–85/15–80/20–75/25–70/30 heterostructure the displacement of the hysteresis loop can be determined, again, from the values given in Fig. 10b by multiplication with (-1). It is also significant to note from Fig. 11 that there is no shift in the hysteresis loops of ferroelectric heterostructures free from space charges regardless whether they are upgraded or downgraded.

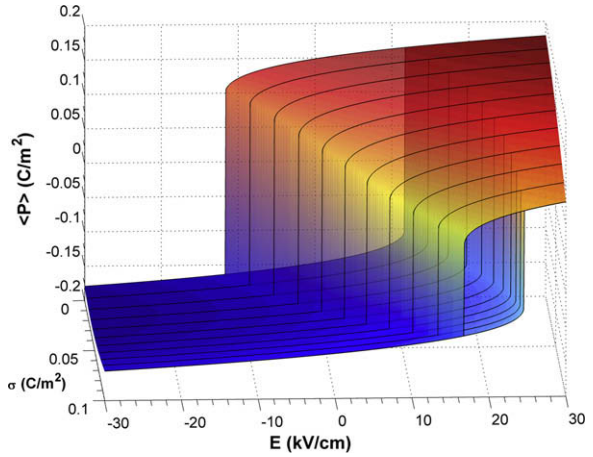

Fig. 9. Dependence of the hysteresis loop of five-layered upgraded BST 70/30–75/25–80/20–85/15–90/10 heterostructure on symmetrically distributed σ at room temperature.

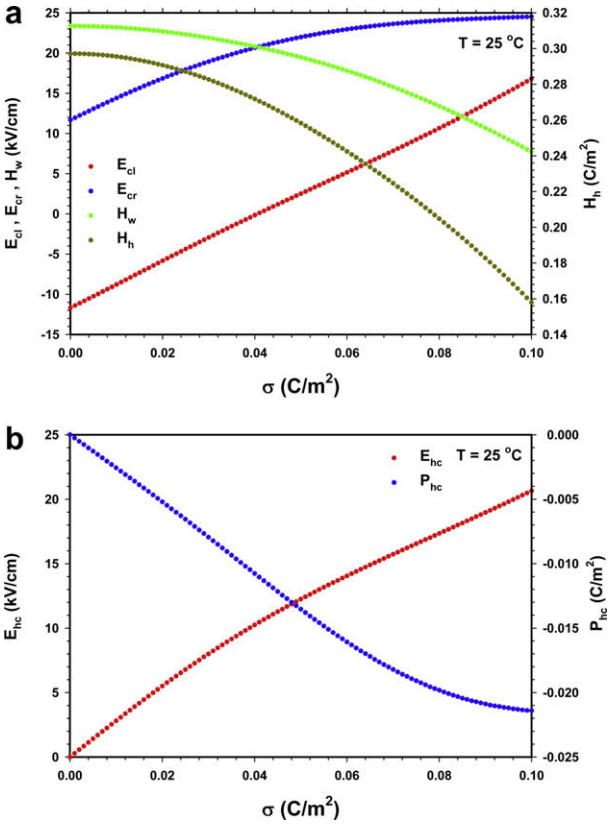

Fig. 10. Dependence of the hysteresis parameters of five-layered upgraded BST 70/30–75/25–80/20–85/15–90/10 heterostructure on symmetrically distributed σ at room temperature.

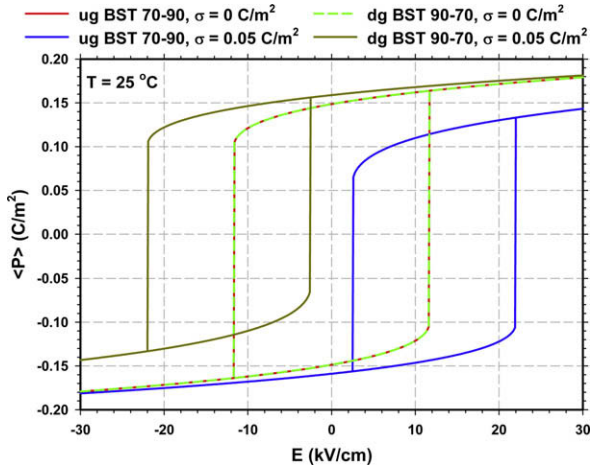

Fig. 11. Room temperature hysteresis loops of five-layered upgraded (ug) BST 70/30–75/25–80/20–85/15–90/10 and downgraded (dg) BST 90/10–85/15–80/20–75/25–70/30 heterostructures with symmetrically distributed σ.

We further investigated the asymmetry of the polarization response in a five-layered upgraded BST 70/30–75/25–80/20–85/15–90/10 heterostructure. In the absence of an externally applied electric field, $E^{ext} = 0$, the dependence of both average positive (up) and average negative (down) polarizations on temperature T and space charge density σ are plotted in Fig. 12a–c. At $\sigma = 0$ C m^{-2}, the average positive and average negative polarization values are symmetric, i.e. $\langle P_{positive} \rangle = |\langle P_{negative} \rangle|$. This symmetry is lost when even minor amounts of interfacial charges are introduced into the heterostructure (Fig. 12a and b). It can be clearly seen that the ferroelectric transition temperature is suppressed as the space charge density is increased (Fig. 12c). This is in complete agreement with the results of Bratkovsky and Levanyuk for simple monolithic ferroelectric bilayers [19]. Additionally, there is a nonzero polarization in the paraelectric region that can be explained due to presence of space charges in the heterostructure, as illustrated in Fig. 12a–c. This is the built-in, nonswitchable

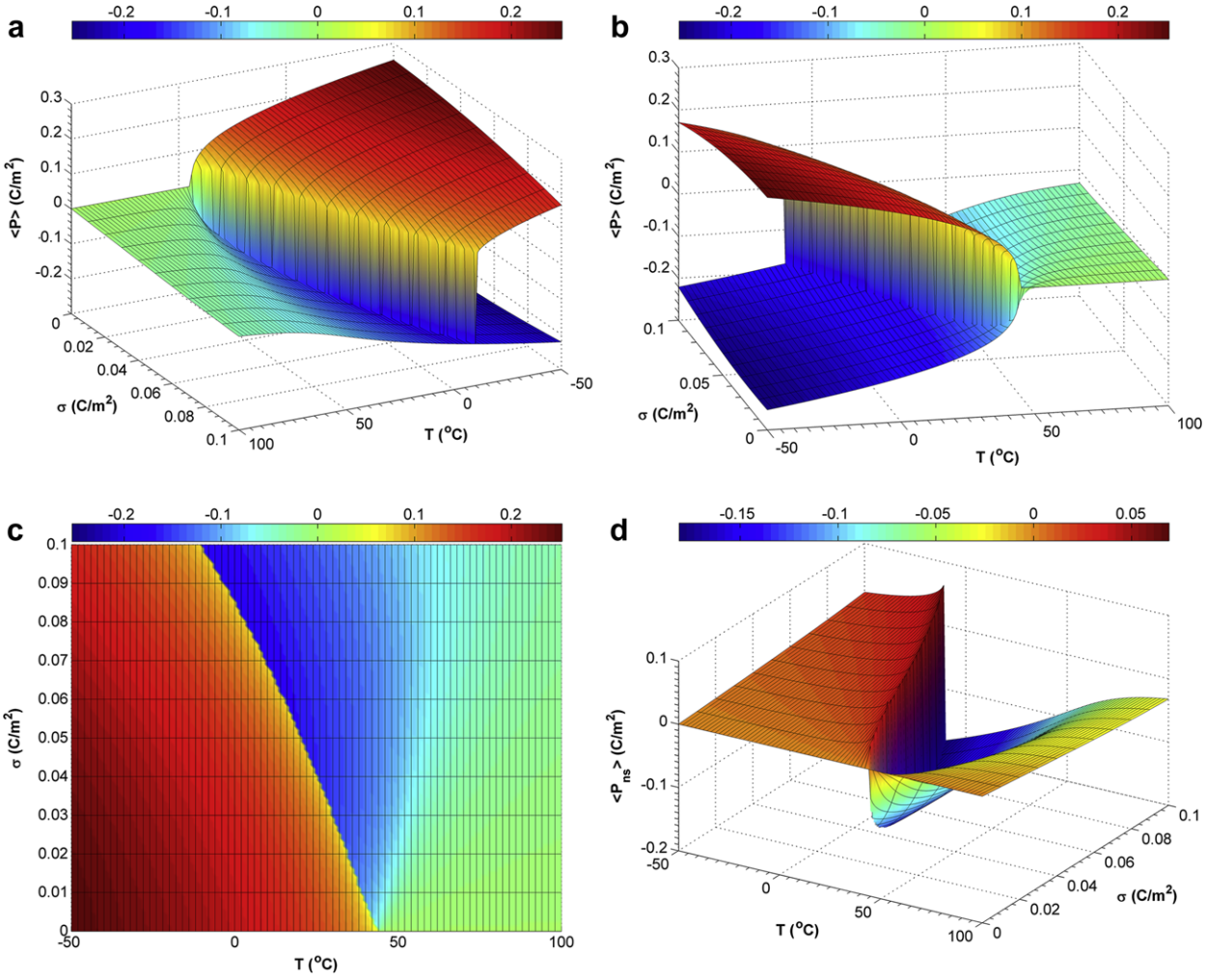

Fig. 12. (a–c) Three-dimensional plots of the average equilibrium polarization (both positive and negative) as a function of the temperature and σ in a five-layered upgraded BST heterostructure with compositions from the bottom layer to the top layer corresponding to BST 70/30–75/25–80/20–85/15–90/10 at $E^{ext} = 0$. (d) The average built-in (nonswitchable) polarization.

polarization of the space charge that exists within the ferroelectric region as well. Thus, the average up/down polarization in the ferroelectric region is actually the sum of two different polarizations: namely (i) the average built-in (nonswitchable) polarization $\langle P_{ns} \rangle$ and (ii) average ferroelectric (switchable) polarization $\langle P_{sw} \rangle$. We plot the variation of the average built-in polarization in the ferroelectric heterostructure in Fig. 12d. Within the ferroelectric region, the built-in polarization *always* corresponds to a metastable state of the ferroelectric heterostructure compared to the up/down ferroelectric polarizations. Furthermore, although not shown here, note that the built-in polarization in each layer is sensitive to temperature changes in compositionally graded multilayers whereas in monolithic ferroelectrics with space charges (see Section 3.2) there is no such a temperature dependency of the built-in polarization as discussed by Bratkovsky and Levanyuk [19].

The (total) polarization $P_i = P_{ns,i} + P_{sw,i}$ of each layer in the absence of an externally applied electric field as a function of σ at 0 °C and 25 °C are shown in Fig. 13. At $T = 0$ °C, in the ferroelectric regime ($\sigma < 0.086$ C m^{-2}), higher (total) polarization P_i values are attained in ferroelectrically softer compositions whereas in the paraelectric region this behavior is completely reversed. As expected, the polarization P_i varies considerably from the average polarization $\langle P \rangle$ with increasing space charge density. An interesting polarization state arises in the ferroelectric heterostructure in the vicinity of $\sigma \approx 0.084$ C m^{-2}. It seems that there is an anti-ferroelectric interaction across the interlayer interfaces between BST 90/10 and BST 85/15, i.e. the (total) polarization in BST 90/10 is negative whereas it is positive in BST 85/15 and other layers. The switchable (ferroelectric) polarization P_{sw} in each layer is practically the same, as shown in Fig. 13c, although there is a difference of $\approx 10^{-3}$–10^{-4} C m^{-2} between adjacent layers. The highest switchable polarization, P_{sw}, exist in the layer having the ferroelectrically "hardest" composition, BST 90/10. At $T = 25$ °C, the ferroelectric to paraelectric transition takes place at a lower charge density ($\sigma = 0.04$ C m^{-2}) and, with the exception of the anti-ferroelectric coupling between layers, all the features of P_i, P_{ns}, and P_{sw} mentioned for $T = 0$ °C are the same.

We note that the formalism presented in this study is based on thermodynamics and as such it cannot account for dynamic effects resulting from migration of space charges [15,31]. Furthermore, the switching of the ferroelectric multilayers discussed herein corresponds to thermodynamic instability rather than nucleation and growth of electrical domains. Other mechanisms that have not been considered include stresses at the surfaces or electrode

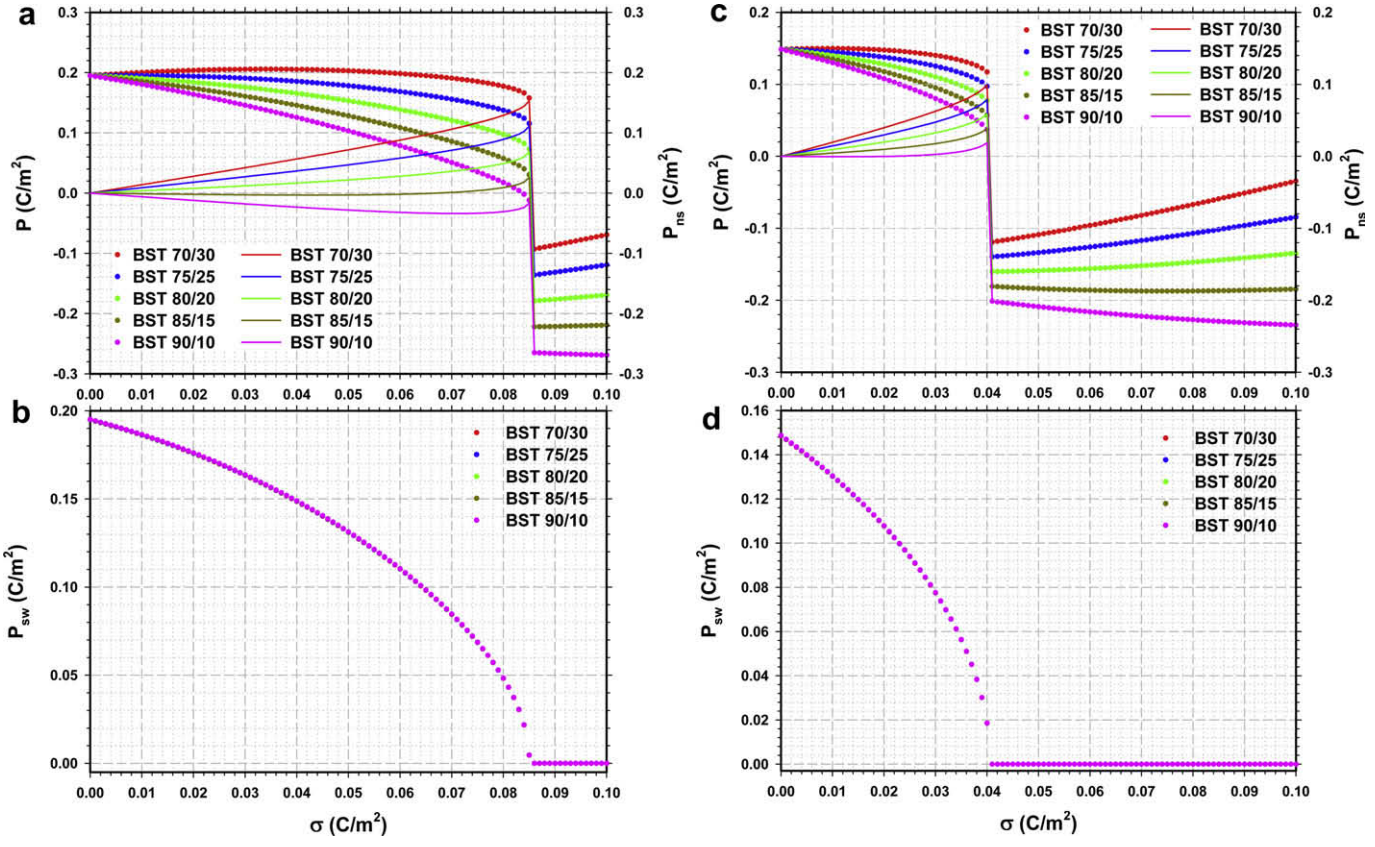

Fig. 13. The variation of the total equilibrium polarization, P, nonswitchable (built-in) polarization P_{ns} (solid line) and switchable (ferroelectric) polarization P_{sw} in a five-layered upgraded BST 70/30–75/25–80/20–85/15–90/10 heterostructure in each layer at $E^{ext} = 0$: (a and b) at $T = 0$ °C; (c and d) at $T = 25$ °C.

interfaces [32] that may be greater than the electrostatic effects and possible intervening effects resulting from electrode screening and/or metal induced gap states [33]. However, the theoretical results identify the origin of the role of space charges and compositional gradients and establish the driving force for the behavior of such materials when an electric field is applied. Therefore, these findings can be employed to design multilayer ferroelectric materials systems for sensors/actuators and tunable devices by exploiting the electrostatic interlayer interactions.

4. Conclusions

In this study, we have analyzed the equilibrium polarization states and corresponding thermodynamic hysteresis loops of monolithic/multilayer ferroelectrics under the combined effect of compositional grading and localized space charges. The theoretical model was based on a non-linear thermodynamic approach using Landau theory of phase transformations and incorporating electrostatic interactions arising from the presence of both "built-in" and "switchable" polarizations. Our numerical results show that for stress-free compositionally graded BST multilayers there is a diagonal off-set of the polarization hysteresis loops corresponding to a displacement along both the applied field and polarization axes only if there are both localized space charges and compositional gradients in the heterostructure. While the present study correctly identifies the driving force for polarization reversal in such constructs, future work should concentrate on dynamic properties of these materials systems, including possible domain mechanisms and defect mobility.

Acknowledgement

The work at UConn was supported by the US Army Research Office through Grants W911NF-05-1-0528 and W911NF-08-C-0124.

Appendix A

The system of equations given by relations (1) and (2) are solved as follows:

$$\begin{bmatrix} 1 & -1 & 0 & 0 & \cdots & 0 & 0 \\ 0 & 1 & -1 & 0 & \cdots & 0 & 0 \\ 0 & 0 & 1 & -1 & \cdots & 0 & 0 \\ \vdots & \vdots & \vdots & & & \vdots & \vdots \\ 0 & 0 & 0 & 0 & \ddots & -1 & 0 \\ 0 & 0 & 0 & 0 & \cdots & 1 & -1 \\ \ell_1 & \ell_2 & \ell_3 & \ell_4 & \cdots & \ell_{n-1} & \ell_n \end{bmatrix} \begin{vmatrix} E_{D,1} \\ E_{D,2} \\ E_{D,3} \\ \vdots \\ E_{D,n-2} \\ E_{D,n-1} \\ E_{D,n} \end{vmatrix} = -\frac{1}{\varepsilon_0} \begin{vmatrix} P_1 - P_2 - \sigma \\ P_2 - P_3 - \sigma \\ P_3 - P_4 - \sigma \\ \vdots \\ P_{n-2} - P_{n-1} - \sigma \\ P_{n-1} - P_n - \sigma \\ 0 \end{vmatrix} \tag{A1}$$

The augmented matrix of Eq. (A1),

$$\left[\begin{array}{ccccccc|c} 1 & -1 & 0 & 0 & \cdots & 0 & 0 & -(P_1 - P_2 - \sigma)/\varepsilon_0 \\ 0 & 1 & -1 & 0 & \cdots & 0 & 0 & -(P_2 - P_3 - \sigma)/\varepsilon_0 \\ 0 & 0 & 1 & -1 & \cdots & 0 & 0 & -(P_3 - P_4 - \sigma)/\varepsilon_0 \\ \vdots & \vdots & \vdots & & & \vdots & \vdots & \vdots \\ 0 & 0 & 0 & 0 & \ddots & -1 & 0 & -(P_{n-2} - P_{n-1} - \sigma)/\varepsilon_0 \\ 0 & 0 & 0 & 0 & \cdots & 1 & -1 & -(P_{n-1} - P_n - \sigma)/\varepsilon_0 \\ \ell_1 & \ell_2 & \ell_3 & \ell_4 & \cdots & \ell_{n-1} & \ell_n & 0 \end{array}\right] \tag{A2}$$

can be rewritten after a simple Gaussian elimination as:

$$\left[\begin{array}{ccccccc|c} 1 & -1 & 0 & 0 & \cdots & 0 & 0 & -(P_1 - P_2 - \sigma)/\varepsilon_0 \\ 0 & 1 & -1 & 0 & \cdots & 0 & 0 & -(P_2 - P_3 - \sigma)/\varepsilon_0 \\ 0 & 0 & 1 & -1 & \cdots & 0 & 0 & -(P_3 - P_4 - \sigma)/\varepsilon_0 \\ \vdots & \vdots & \vdots & & & \vdots & \vdots & \vdots \\ 0 & 0 & 0 & 0 & \ddots & -1 & 0 & -(P_{n-2} - P_{n-1} - \sigma)/\varepsilon_0 \\ 0 & 0 & 0 & 0 & \cdots & 1 & -1 & -(P_{n-1} - P_n - \sigma)/\varepsilon_0 \\ 0 & 0 & 0 & 0 & \cdots & 0 & \sum_{i=1}^{n} \ell_i & \frac{1}{\varepsilon_0}\left[\sum_{i=1}^{n-1}\left(\sum_{j=1}^{i} \ell_j\right)(P_i - P_{i+1} - \sigma)\right] \end{array}\right] \tag{A3}$$

The last summation term can be expressed as:

$$\frac{1}{\varepsilon_0}\left[\sum_{i=1}^{n-1}\left(\sum_{j=1}^{i} \ell_j\right)(P_i - P_{i+1} - \sigma)\right] = -\frac{1}{\varepsilon_0}\left[\left(\sum_{j=1}^{n} \ell_j\right)P_n - \sum_{i=1}^{n} \ell_i P_i + \left(\sum_{i=1}^{n-1}\sum_{j=1}^{i} \ell_j\right)\sigma\right] \tag{A4}$$

Solving for $E_{D,n}$, one finds

$$\left(\sum_{i=1}^{n} \ell_i\right)E_{D,n} = -\frac{1}{\varepsilon_0}\left[\left(\sum_{j=1}^{n} \ell_j\right)P_n - \sum_{i=1}^{n} \ell_i P_i + \left(\sum_{i=1}^{n-1}\sum_{j=1}^{i} \ell_j\right)\sigma\right] \tag{A5}$$

$$E_{D,n} = -\frac{1}{\varepsilon_0}\left[P_n - \sum_{j=1}^{n} \alpha_j P_j + \left(\sum_{i=1}^{n-1}\sum_{j=1}^{i} \alpha_j\right)\sigma\right] \tag{A6}$$

where $\alpha_j = \ell_j / \sum_{i=1}^{n} \ell_i$. For clarification, it is worth to mention that in Eq. (A6) the upper bounds of summations "n" and "$n-1$" are independent from the index "n" given on the left-hand side of the equation. The double summation term in Eq. (A6) can be expressed as a single summation as:

$$\sum_{i=1}^{n-1}\sum_{j=1}^{i} \alpha_j = \sum_{k=1}^{n-1}(n-k)\alpha_k = \sum_{k=1}^{n}(n-k)\alpha_k \tag{A7}$$

Thus,

$$E_{D,n} = -\frac{1}{\varepsilon_0}\left[P_n - \sum_{j=1}^{n} \alpha_j P_j + \left(\sum_{j=1}^{n}(n-j)\alpha_j\right)\sigma\right] \tag{A8}$$

Through back substitution, it is straightforward to show that the solutions of the system of equations given via Eqs. (1) and (2) are

$$E_{D,i} = -\frac{1}{\varepsilon_0}\left[P_i - \sum_{j=1}^{n}\alpha_j P_j + \left(\sum_{j=1}^{n}(n-j)\alpha_j - (n-i)\right)\sigma\right], \quad i = 1, 2, \ldots, n \tag{A9}$$

References

[1] Schubring NW, Mantese JV, Micheli AL, Catalan AB, Lopez RJ. Phys Rev Lett 1992;68:1778.
[2] Bao D, Lee SK, Zhu X, Alexe M, Hesse D. Appl Phys Lett 2005;86:082906.
[3] Bao D, Mizutani N, Yao X, Zhang L. Appl Phys Lett 2000;77:1041.
[4] Bao D, Wakiya N, Shinozaki K, Mizutani N, Yao X. J Appl Phys 2001;90:506.
[5] Boerasu I, Pintilie L, Kosec M. Appl Phys Lett 2000;77:2231.
[6] Brazier M, McElfresh M, Mansour S. Appl Phys Lett 1999;74:299.
[7] Sigman J, Clem PG, Nordquist CD. Appl Phys Lett 2006;89:132909.
[8] Zhu X, Zhu J, Zhou S, Liu Z, Ming N, Chan HL-W, et al. Mater Sci Eng B-Solid 2005;118:219.
[9] Bao D, Yao X, Zhang L. Appl Phys Lett 2000;76:2779.
[10] Cole MW, Ngo E, Hirsch S, Okatan MB, Alpay SP. Appl Phys Lett 2008;92:072906.
[11] Cole MW, Ngo E, Hirsch S, Demaree JD, Zhong S, Alpay SP. J Appl Phys 2007;102:034104.
[12] Fellberg W, Mantese J, Schubring N, Micheli A. Appl Phys Lett 2001;78:524.
[13] Mantese JV, Schubring NW, Micheli AL, Thompson MP, Naik R, Auner GW, et al. Appl Phys Lett 2002;81:1068.
[14] Bouregba R, Poullain G, Vilquin B, Rhun GL. J Appl Phys 2003;93:5583.
[15] Chan HK, Lam CH, Shin FG. J Appl Phys 2004;95:2665.
[16] Henisch HK. Semiconductor contacts: an approach to ideas and models. Oxford: Clarendon Press; 1984.
[17] Marvan M, Fousek J. Phase Transit 2006;79:485.
[18] Bratkovsky AM, Levanyuk AP. Phys Rev Lett 2005;94:107601.
[19] Bratkovsky AM, Levanyuk AP. Phys Rev B 2000;61:15042.
[20] Zubko P, Jung DJ, Scott JF. J Appl Phys 2006;100:114112.
[21] Zubko P, Jung DJ, Scott JF. J Appl Phys 2006;100:114113.
[22] Pintilie L, Vrejoiu I, Hesse D, LeRhun G, Alexe M. Phys Rev B 2007;75:104103.
[23] Okatan MB, Cole MW, Alpay SP. J Appl Phys 2008;104:104107.
[24] Misirlioglu IB, Alexe M, Pintilie L, Hesse D. Appl Phys Lett 2007;91:022911.
[25] Roytburd AL, Slutsker J. Appl Phys Lett 2006;89:042907.
[26] Artemev A, Geddes B, Slutsker J, Roytburd A. J Appl Phys 2008;103:074104.
[27] Pertsev NA, Zembilgotov AG, Tagantsev AK. Phys Rev Lett 1998;80:1988.
[28] Okatan MB, Mantese JV, Alpay SP. Phys Rev B 2009;79:174113.
[29] Warren WL, Dimos D, Pike GE, Tuttle BA, Raymond MV, Ramesh R, et al. Appl Phys Lett 1995;67:866.
[30] Warren WL, Tuttle BA, Dimos D, Pike GE, Al-Shareef HN, Ramesh R, et al. Jpn J Appl Phys 1996;35:1521.
[31] O'Neill D, Bowman RM, Gregg JM. Appl Phys Lett 2000;77:1520.
[32] Luk'yanchuk IA, Schilling A, Gregg JM, Catalan G, Scott JF. Phys Rev B 2009;79:144111.
[33] Dawber M, Chandra P, Littlewood PB, Scott JF. J Phys Condens Matter 2003;15:L393.